On North Pacific Temperature, Salinity, Sound Velocity and Density Fronts and their Relation to the Wind and Energy Flux Fields[1]

GUNNAR I. RODEN

Department of Oceanography, University of Washington, Seattle 98195

(Manuscript received 16 December 1974, in revised form 30 April 1975)

ABSTRACT

The main oceanic fronts of the North Pacific are investigated and the principal frontogenetic processes described. Fronts are features of the upper ocean and occur near mass transport and energy flux convergence zones. Frontogenesis in the upper layers of the ocean is strongly dependent upon the configuration of the wind stress field. Temperature and salinity fronts in the upper ocean are not necessarily coincident, nor are they always accompanied by density fronts. During periods of strong and persistent winds, the upper and lower portions of the front may separate at pycnocline depth by as much as 200 km, suggesting Ekman-type displacement of the upper layer. Multiple temperature and salinity fronts, spaced 60–70 km apart and suggestive of baroclinic Rossby waves, are observed off northeastern Japan at the confluence of the Kuroshio with the Oyashio. Not all temperature and salinity fronts are accompanied by strong baroclinic flow and the maximum baroclinic flow often occurs several kilometers distant from the surface manifestation of these fronts.

1. Introduction

Oceanic fronts differ from the better known atmospheric fronts in several important ways. In the atmosphere, temperature and density fronts almost always coincide and it has been customary to treat the fronts as temperature discontinuities of order zero or one and relate these to dynamic processes via appropriate boundary conditions and the equation of state. The frontal slopes, the presence of cyclonic vorticity in frontal areas, the roll-up of fronts, jet streams, and dynamic instabilities on frontal surfaces have all been investigated theoretically and compared to actual observations, with generally favorable results for the free atmosphere of the extratropical zone (Godske *et al.*, 1957; Palmén and Newton, 1969). Fronts associated with the other atmospheric variable, moisture, have not been investigated as thoroughly. Recent studies include the movement of drylines (Schaefer, 1974) and tropical cyclogenesis (Charney, 1971).

Progress in understanding oceanic fronts has been much slower, because of the difficulty of observation and the inapplicability of much of classical theories developed for the atmosphere. The reason for the latter is that the ocean is a doubly stratified medium, in which the salinity plays a role as important as temperature. Thus, temperature and salinity fronts may, or may not, be accompanied by density fronts. When the thermal and haline fronts point in the same direction, as happens in the subarctic region of the Pacific, density gradients across the frontal zone are weak or nonexistent (Roden, 1972). In tropical latitudes, where the temperature is almost constant, strong density fronts are associated with salinity fronts at the boundaries of the doldrums (Roden, 1974). Moreover, as will be shown below, temperature and salinity fronts have been found to separate, not only horizontally, but also vertically, with the result that the strongest baroclinic flow may occur some distance from the surface manifestation of the temperature or salinity fronts.

The above observational features make it unrealistic to define oceanic fronts in terms of density discontinuities, because such discontinuities are not observed at most fronts. It is necessary also to specify the variable, because the existence of one front does not apply to the existence of others. The approach taken here is to define the respective fronts in terms of the magnitude of gradients and ask what thermodynamic processes are responsible for the strengthening and weakening of fronts.

An initially inhomogeneous medium is necessary for the occurrence of thermohaline fronts. The ocean is rendered inhomogeneous largely by the geographically variable energy fluxes through the sea surface. These set up internal circulations which will concentrate the existing gradients in some places (frontogenesis) and decrease them in others (frontolysis). A knowledge of the configuration of the surface energy flux fields is important, therefore, in studies dealing with frontal dynamics.

[1] Contribution No. 846 from the Department of Oceanography, University of Washington.

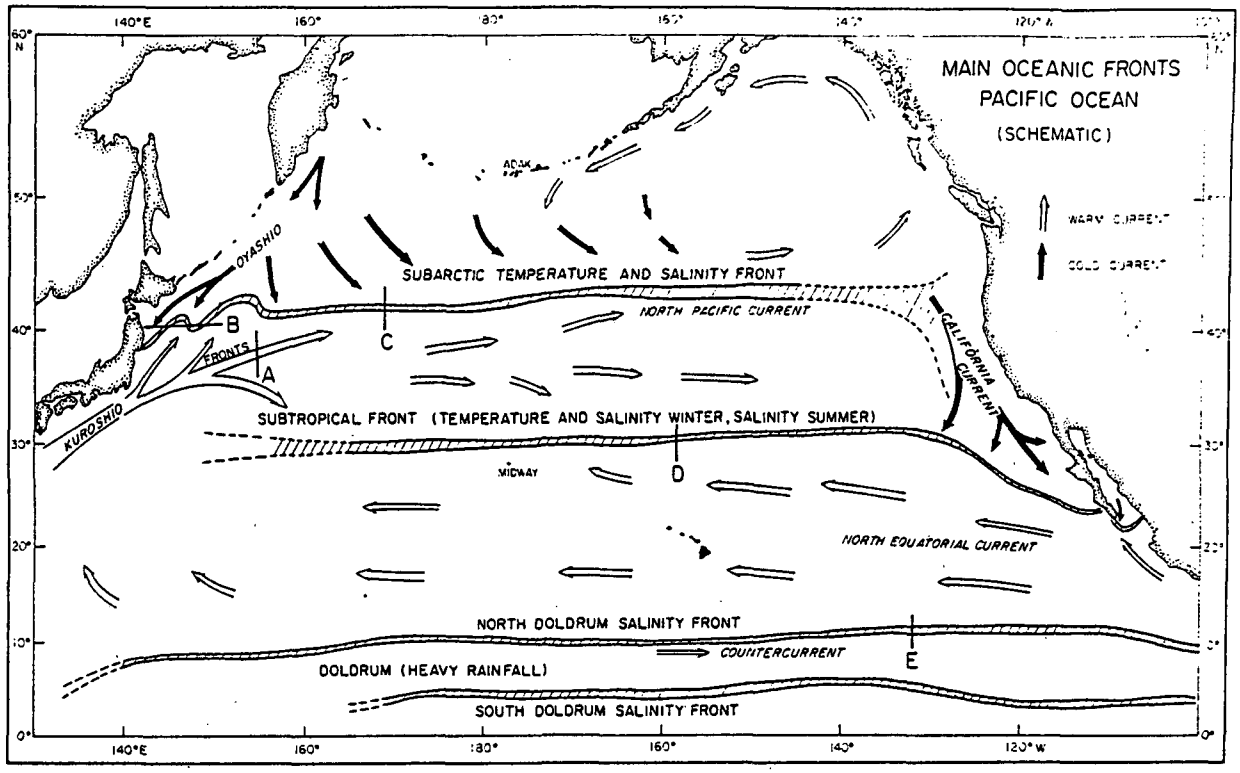

FIG. 1. Schematic map of main North Pacific fronts. Arrows indicate prevailing current directions. Letters refer to fronts shown in Figs. 2–10. A, Kuroshio front; B, Oyashio front; C, subarctic front; D, subtropical front; E, doldrum front.

In the following, a description is given of the observed thermohaline features of the major North Pacific fronts and of the time variations of the important energy flux fields. This is followed by a brief outline of kinematic and dynamic processes to be expected in frontal regions.

The observational evidence of the North Pacific fronts is based on the cruises of the R/V *Thomas G. Thompson*, of the University of Washington, during the years 1968–74. The vertical temperature and salinity structure was measured with the continuously recording Plessey Model 9006 STD and Model 9040 CTD to an accuracy of 0.01°C and 0.03‰, respectively. The sound velocity was computed from Wilson's equation (Vigoureux and Hersey, 1962) using the STD and CTD data as input.

2. Observed thermohaline features of major North Pacific fronts

In the North Pacific, major oceanic fronts occur near the boundaries of planetary wind and current systems. The location of the principal fronts is shown in Fig. 1 and their characteristics, as obtained by horizontal sampling at 30 km intervals and vertical sampling at 3 m intervals, are summarized in Table 1. The outstanding features observed at the major fronts are as follows:

TABLE 1. Characteristics of North Pacific fronts, based on horizontal sampling at 30 km intervals. All gradients are expressed in terms of the Nyquist sampling interval.

Characteristics*	North Pacific fronts				
	Kuroshio	Oyashio	Subarctic	Subtropical	Doldrum
Temperature gradient (°C per 60 km)	6	9	8	4	1
Salinity gradient (‰ per 60 km)	0.6	1.5	1.2	0.5	1.0
Sound velocity gradient (m s^{-1} per 60 km)	24	39	28	12	1
Density gradient (kg m^{-3} per 60 km)	0.8	0.2	0.2	0.8	0.7
Baroclinic current (m s^{-1})	0.6	0.2	0.4	0.5	0.5
Baroclinic shear (s^{-1})	2×10^{-5}	8×10^{-6}	7×10^{-6}	10^{-5}	2×10^{-5}

* Maximum values.

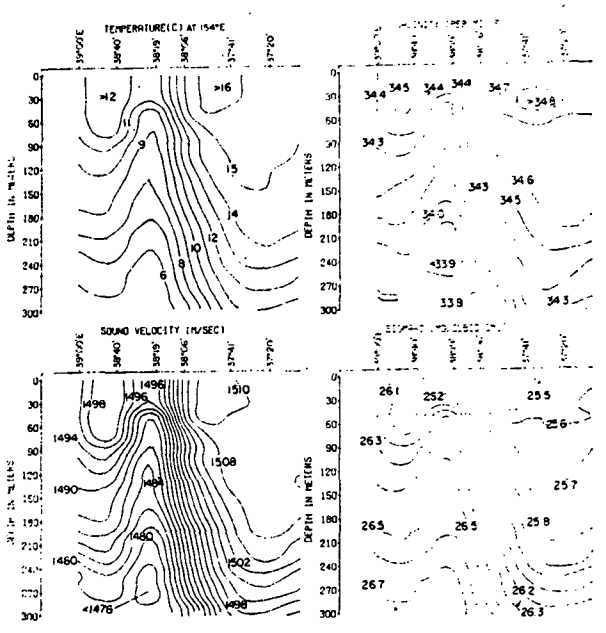

FIG. 2. Temperature, salinity, sound velocity and density sections across the Kuroshio front at longitude 154°E. The sections were occupied on 24 April 1971.

a. Kuroshio front (Fig. 2 and 3, left)

This front results from the intrusion of warm and high salinity water carried poleward by the fast flowing Kuroshio. The horizontal thermohaline gradients are most pronounced at the northern edge of this current and can be traced from Japan several thousand kilometers seaward (Kawai, 1972). The front is vertical in the upper 50 m and slopes slightly to the southward between 50 and 300 m. Strong baroclinity is encountered at the front, with large positive vorticity on the south side of the current. The Kuroshio front comes closest to resembling classical atmospheric fronts.

The path of the Kuroshio is subject to many meanders, the larger ones of which have been investigated by Uda (1935, 1938, 1963) and Taft (1972). By implication the Kuroshio front can be expected to show similar meandering. Detailed investigations of the meanders are lacking, but evidence for it is suggested in the 10-day surface temperature maps published regularly by the Japan Meteorological Agency (1970–74).

b. Oyashio fronts (Figs. 4, 5 and 6)

In the sea area of northeastern Japan, where branches of the cold and low salinity Oyashio intermingle with offshoots from the warm and high salinity Kuroshio, numerous fronts are found (Uda, 1938; Masuzawa, 1957; Kawai, 1972). Recent field investigations by the author aboard the *Thomas G. Thompson* have revealed the existence of multiple and nearly equally spaced fronts. On a 400 km long section, taken along latitude 40°N, between the coast of Japan and longitude 147°E in late April 1971, six thermohaline fronts, spaced about 60–70 km apart were found. The spacing is of the order of the cutoff wavelength for baroclinic Rossby waves in a two-layer ocean (Longuet-Higgins, 1965). Waves having such length scales have been implicated in theories dealing with baroclinic instability in the ocean (Tareev, 1965; Pedlosky, 1971).

It is noteworthy that while the Oyashio fronts are characterized by strong horizontal temperature, salinity and sound velocity gradients, the horizontal density gradients are rather weak. Thus, no strong baroclinic flow is found at these fronts. On the other hand, the baroclinic shear between the oppositely flowing current branches is large, suggesting strong vorticity.

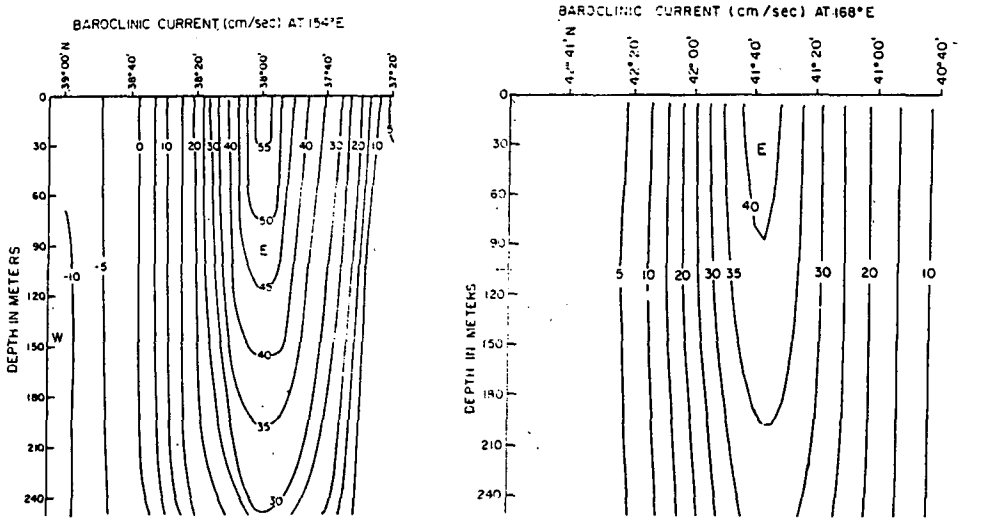

FIG. 3. Baroclinic flow, relative to 1500 db, at the Kuroshio front at longitude 154°E (left) and at the subarctic front at longitude 168°E (right).

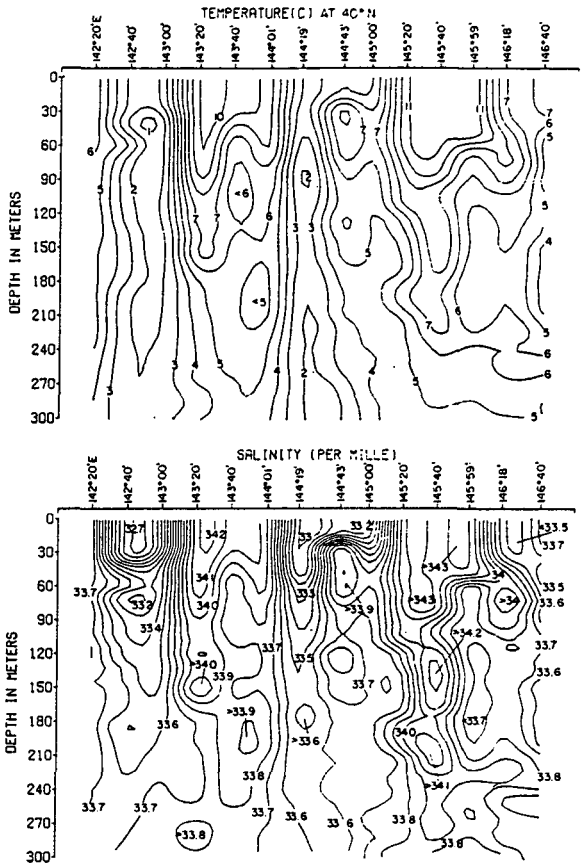

FIG. 4. Temperature and salinity sections across the Oyashio fronts at latitude 40°N. The sections were occupied on 28 and 29 April 1971.

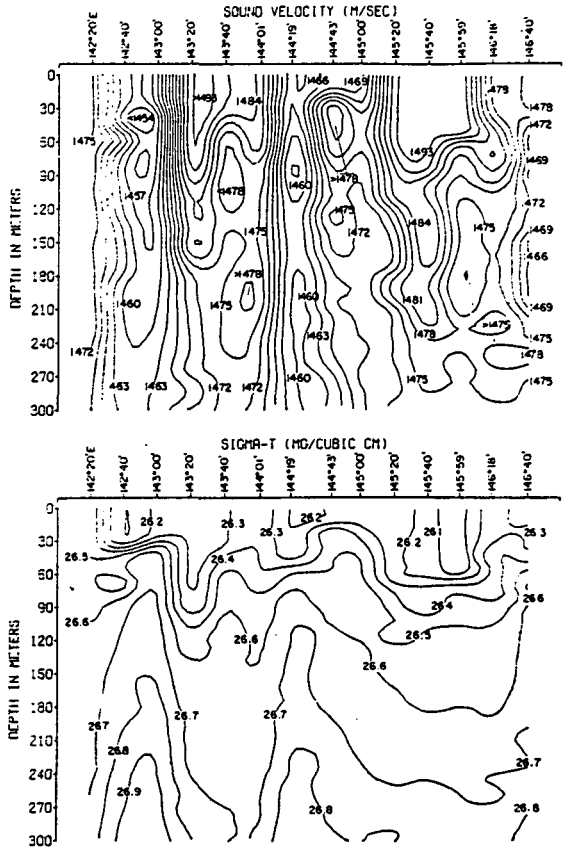

FIG. 5. Sound velocity and density sections across the Oyashio fronts at latitude 40°N.

c. *Subarctic front* (Figs. 3, right, and 7)

This front is normally encountered in the latitude range between 40 and 45°N and is strongly influenced by the wind field. In the central North Pacific, the front appears south of the west wind maximum, in the convergence zone of the southward Ekman transports (Roden, 1970, 1972). In the western Pacific, the subarctic front is influenced, additionally, by the Kuroshio Extension. Particularly large thermohaline gradients are observed where the Ekman transport convergence zone coincides with the northern edge of the Kuroshio Extension.

The subarctic front differs from the Kuroshio front by the absence of a density front in the upper 100 m. Here, an almost complete balance exists between the strong horizontal temperature and salinity gradients. Below 100 m, no such balance is observed and a density front of moderate intensity is found. This density front slopes slightly to the southward. The region of strongest surface baroclinic flow therefore occurs somewhat to the south of the surface temperature and salinity fronts (50 km in the case shown).

A further interesting feature of the subarctic front is the change in mixed layer depth across the front. To

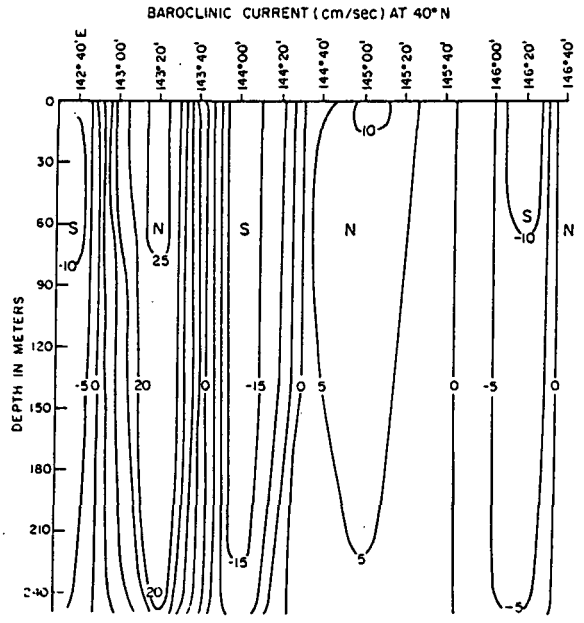

FIG. 6. Baroclinic flow, relative to 1500 db, at the Oyashio fronts at latitude 40°N.

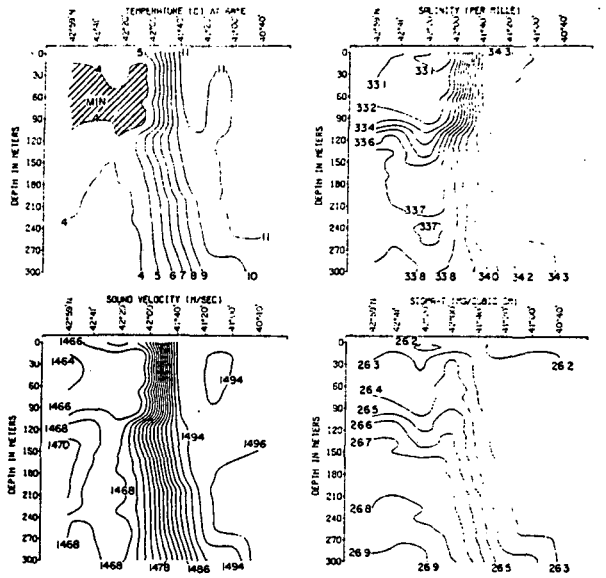

FIG. 7. Temperature, salinity, sound velocity and density sections across the subarctic front at longtiude 168°E. The sections were occupied on 3 and 4 April 1971.

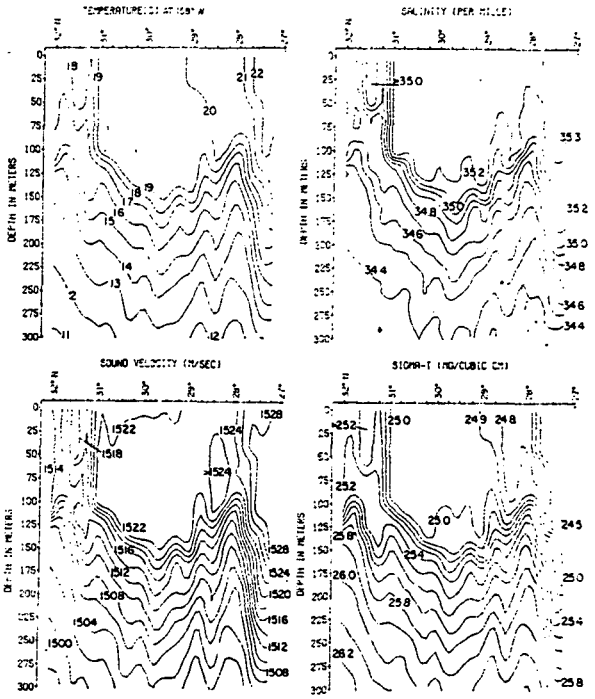

FIG. 8. Temperature, salinity, sound velocity and density sections across the subtropical front at longitude 158°W. The sections were occupied between 25 and 27 January 1974.

the north, the mixed layer extends to the top of the halocline at about 100 m. To the south, the halocline is absent and the mixed layer during the stormy winter and spring months extends to almost 300 m. During the summer months, the mixed layer is determined by the seasonal thermocline, and the contrast across the subarctic front is less (Dodimead *et al.*, 1963).

d. Subtropical fronts (Figs. 8 and 9 left)

These fronts depend strongly upon the wind and energy flux fields at the sea surface. In the central North Pacific, the subtropical fronts occur in the region between the westerlies and the easterly trade winds, in the zone of Ekman transport convergence, roughly along the axis of the North Pacific high pressure ridge. Because the energy flux through the sea surface is also strongly dependent upon the wind, wind boundaries and energy flux boundaries often coincide (Roden, 1974). In the eastern North Pacific, the position of the subtropical fronts is further influenced by the confluence of the cool and low salinity California current with the warm and high salinity north equatorial current. Thus, the subtropical front, located between latitudes 28 and 35°N in the central North Pacific, curves southeastward at the longitude of about 140°W, until it reaches the southern tip of Baja California.

The subtropical front changes considerably with season, from a temperature and salinity front in winter and spring to a salinity front only in summer and fall. These seasonal changes are pronounced in the upper 100 m, the layer above the hydrostatic stability maximum, and become rather negligible below. Above the high stability layer, strong nonconservative processes act upon the moving water particles such that thermal and haline fronts are not always coincident. Below the high stability layer, temperature and salinity fronts usually coincide.

During periods of strong and persistent winds, the upper and lower parts of the subtropical front have a tendency to separate. This is shown in Fig. 8, where the salinity front above the high stability layer is almost 200 km distant from the front beneath this layer. During the period this section was occupied by the *Thomas G. Thompson* in January 1974, and for a week prior to that, strong easterly winds had been blowing.

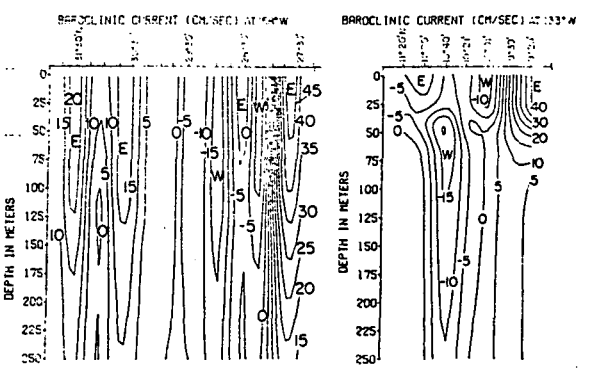

FIG. 9. Baroclinic flow, relative to 1500 db, at the subtropical front at longitude 158°W (left) and at the doldrum front at longitude 133°W (right).

This suggests that the upper mixed layer has been displaced northward by Ekman transport.

The separation of the upper and lower parts of the front leads to the interesting fact that the strongest baroclinic flow (relative to 1500 db) is not found at the location of the surface front, but 200 km to the southward, where the subsurface density front is located. The strong speeds encountered at latitude 28°N are suggestive of the subtropical countercurrent postulated by Yoshida and Kidokoro (1967) and Uda and Hasunuma (1969).

e. Doldrum fronts (Figs. 9, right, and 10)

These fronts are associated with both wind and energy flux boundaries at the limits of the atmospheric intertropical convergence zone (Roden, 1974). The doldrums found are encountered between latitudes 6 and 11°N and are quite shallow, seldom deeper than 40 m. Both salinity and density fronts are found, but no temperature or sound velocity fronts. Because the deeper isopycnals slope upward toward the equator, the strongest baroclinic flow is not found at the surface density front, but almost 180 km to the southward. At the front, the baroclinic current structure is rather complex, consisting of a shallow eastward drift and a faster westward setting undercurrent. The maximum baroclinic velocity shear in the frontal region is of the same order of magnitude as the planetary vorticity, suggesting inertial instability (Van Mieghem, 1951).

3. Temporal variations of fronts deduced from changes in the wind and energy flux fields

Frontogenesis in the ocean is strongly dependent upon the momentum, heat and salt flux fields at the sea surface. These fields change with time and it is of interest to look at the seasonal as well as nonseasonal variations. In the following discussion, the time changes in the central North Pacific are emphasized, because of the availability of data and the absence of strong boundary currents.

a. The field of surface Ekman transports

In mid-ocean the frontogenetic regions can be delineated from a knowledge of the temperature and salinity distributions and the configuration of the wind stress field. The latter is used to calculate the field of surface Ekman transport. Frontogenesis will reach a maximum where strong Ekman transport convergence occurs in a region of large horizontal thermohaline gradients.

The seasonal variation of the surface Ekman transport is shown in Fig. 11, where the arrows indicate the direction of transport. The figure is based on Northern Hemisphere sea level atmospheric pressure maps (National Weather Service, 1957–66), from which the stress of the geostrophic wind and the resulting transports were obtained for a 1° latitude-longitude grid by methods outlined earlier (Roden, 1974).

The seasonal migration of the subtropical convergence zone is clearly indicated. During winter, the 10-year average position of the convergence zone is between latitudes 23 and 28°N. During spring and fall, it is between 32 and 35°N and during summer, it is found between 34 and 37°N. The long-term average orientation of the convergence zone is predominantly zonal. Maximum temperature frontogenesis occurs in spring, when the convergence zone is located in a region of large meridional temperature gradients. Maximum salinity frontogenesis occurs in spring and fall when the convergence zone coincides with the zone of large meridional salinity gradients.

The nonseasonal variations of the surface Ekman transport are shown in Fig. 12, where the arrows indicate the direction of transport and where the filled-in circles refer to fronts observed during the *Thomas G. Thompson* cruise between 18 January and 10 February, 1974. The outstanding feature is that the displacements of the convergence zones during a four-week period in winter are as large as the long-term seasonal displacements. This is associated with the very variable winter weather. During the week of 14–20 January, the mid-Pacific was dominated by large and intense low pressure cells and the convergence zone was between 16 and 19°N, far to the south of its average January position (and the operating area of the research vessel). During the following three weeks, intense low pressures persisted west of the Hawaiian islands, while to the northeast of these islands a strong persistent high pressure center became established. This resulted in a predominantly northeastward orientation of the convergence zone. In the east, the zone was about 8° north of its 10-year average position. The observed fronts all occurred near the convergence zone, which stresses the importance of the configuration of the Ekman transport field in frontal dynamics.

b. The field of net radiative flux

This field is important, because it leads to the establishment of primary temperature gradients in the ocean upon which the flow field subsequently acts to produce regional frontogenesis and frontolysis. The radiation flux field consists essentially of two parts, one of which is astronomical in origin and the other meteorological. On a cloudless earth, the diurnal and seasonal fluctuations of the radiative flux over a uniform water surface would depend chiefly upon the altitude and declination of the sun (Kondratyev, 1969; Budyko, 1974). In mid-ocean, the gradients of the radiative flux would be meridional and likewise vary with the position of the sun. On the real earth, these primary cycles of radiative flux are considerably modified by clouds. The instantaneous cloud fields, as revealed by satellite photographs, are rarely of simple shape, but seem to consist

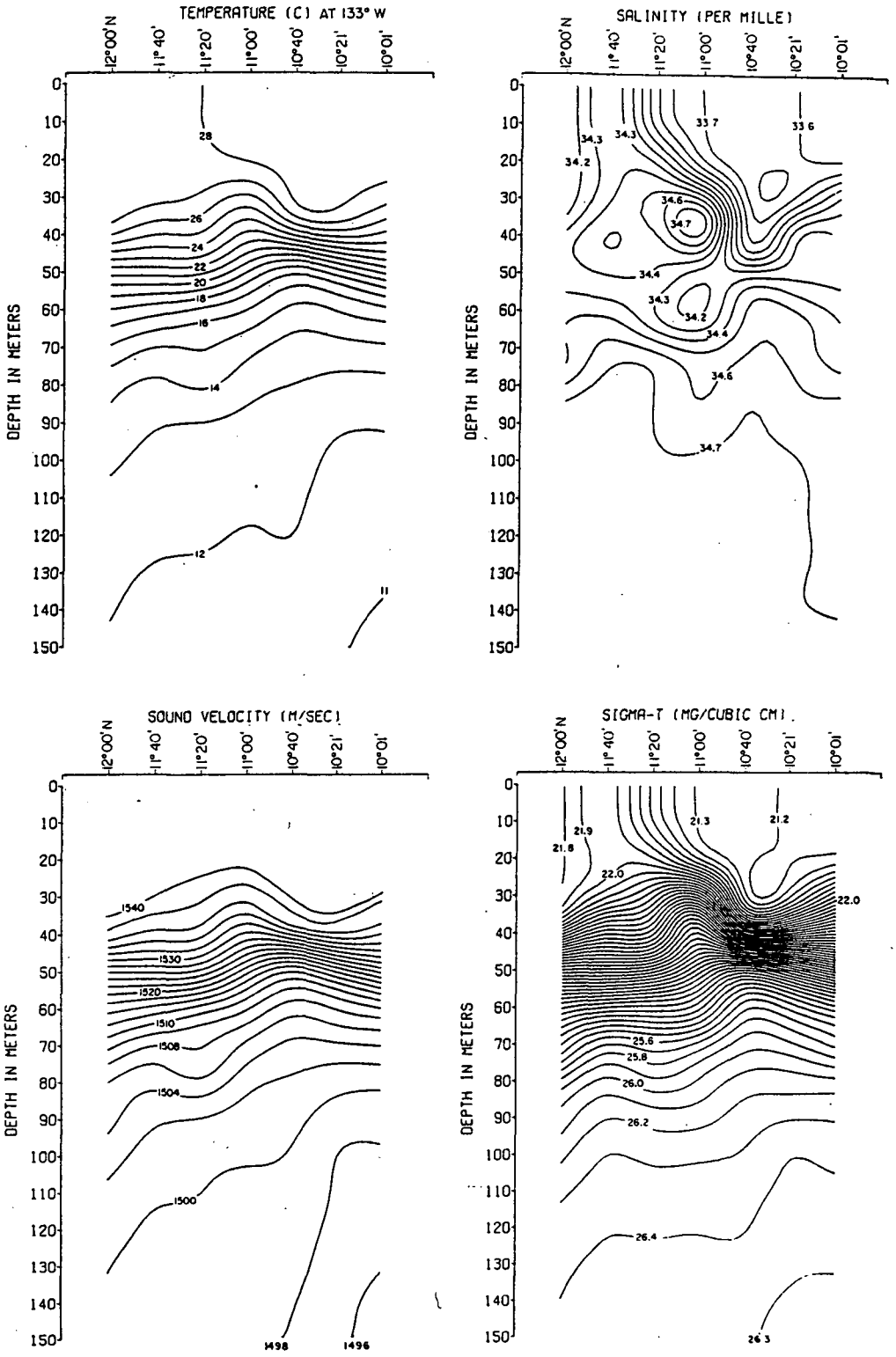

FIG. 10. Temperature, salinity, sound velocity and density sections across the doldrum front at longitude 133°W. The sections were occupied on 18 and 19 October 1972.

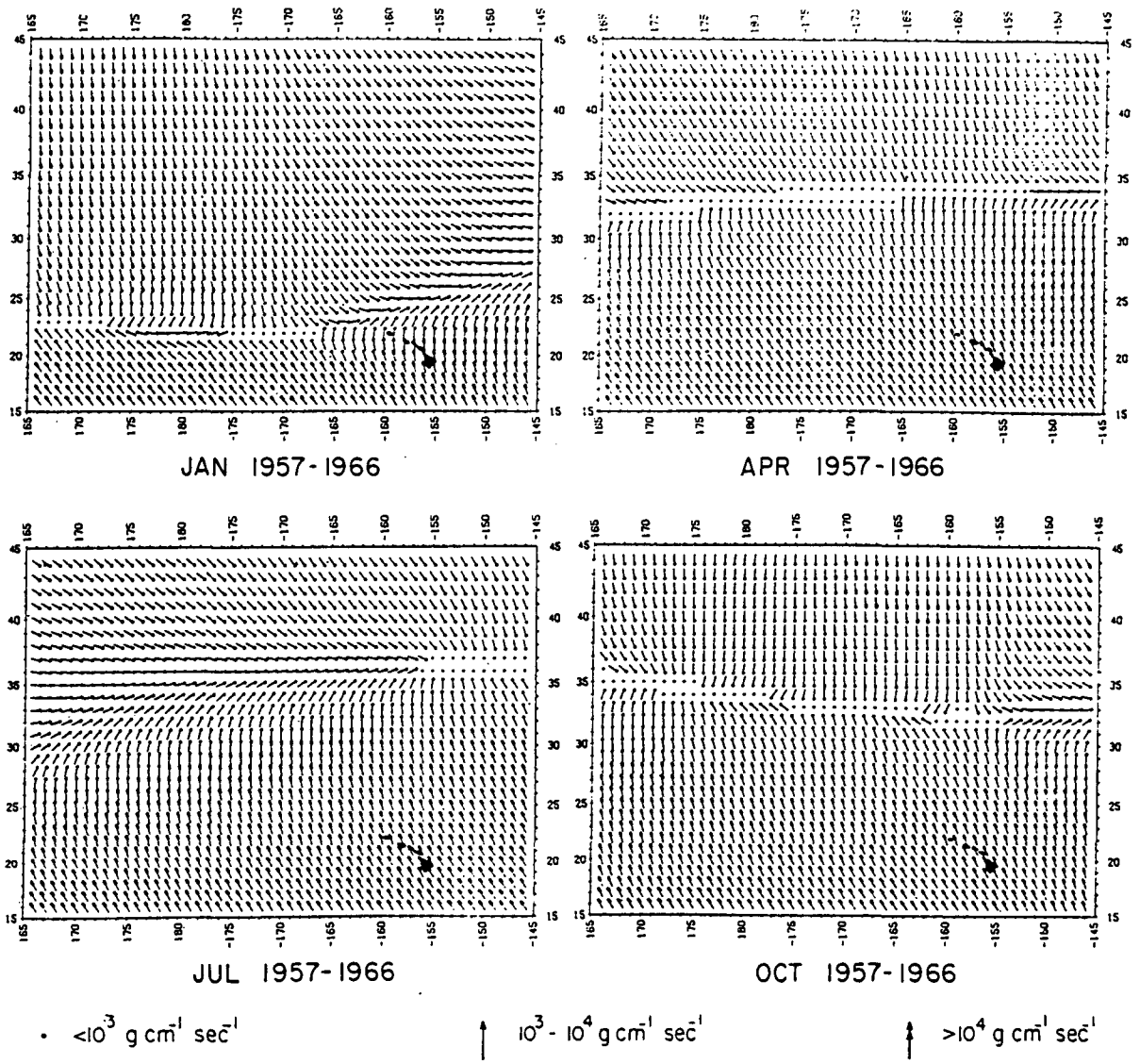

FIG. 11. Seasonal variation of the spatial distribution of the surface Ekman transport on a 1° latitude-longitude grid, based on the stress of the geostrophic wind. Arrows indicate the direction of transport.

of bands, shields and clusters. The time-averaged satellite cloud fields are simpler and show broad regions of cloudiness, separated by large areas that are comparatively clear (Miller, 1971). The change from cloudy to clear regions is often abrupt, indicating the existence of cloud fronts. Maximum radiative flux gradients can be expected in those regions where the cloud fronts coincide with zones of largest astronomically caused radiation gradients.

The seasonal variation of the net radiative flux field in the central North Pacific is shown in Fig. 13. The figure is based on the average satellite cloud cover (Miller, 1971), the average dewpoint and air temperature (Crutcher and Meserve, 1970) and the average sea surface temperature (National Marine Fisheries Service, 1948–67), all evaluated for a 1° latitude-longitude grid. The seasonal variation of the radiative flux is clearly indicated, and depends strongly upon latitude. In the south, the flux is two times larger in summer than in winter. In the north, it is ten times larger.

Areas favorable for temperature frontogenesis can be delineated by superposition of the Ekman transport and net radiation fields (Figs. 11 and 13). During winter, temperature frontogenesis is most likely to occur between latitude 23 and 28°N. During spring and fall, the favorite zone is between 30 and 35°N, and in summer between 35 and 40°N. The rather uniform radiation field south of latitude 30°N in summer will inhibit temperature frontogenesis even in the presence of Ekman transport convergence. This is also observed, as tem-

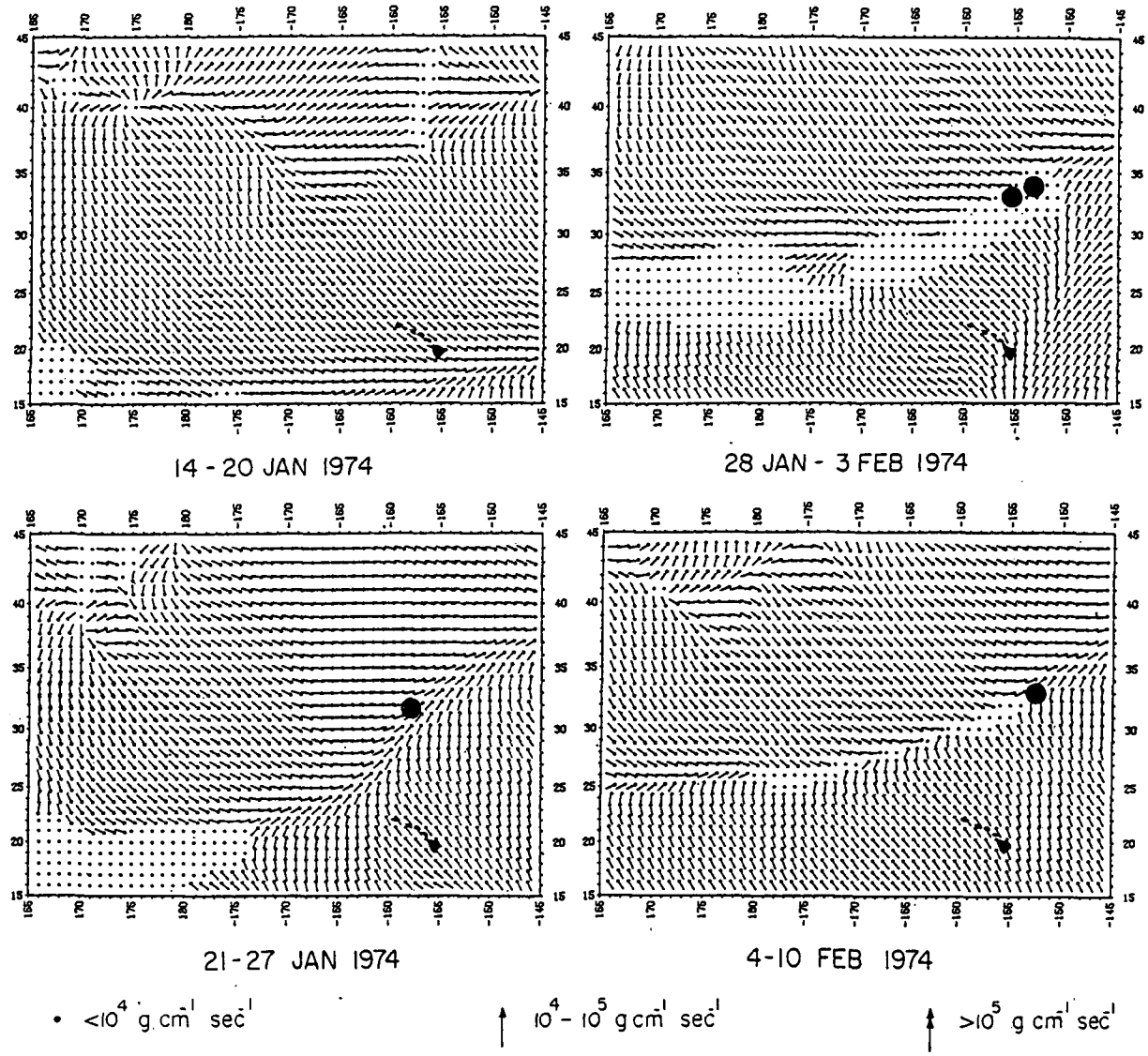

FIG. 12. As in Fig. 11 except for nonseasonal variation. Filled-in circles denote fronts observed on the *Thomas G. Thompson*, 18 January to 10 February, 1974.

perature fronts are nonexistent in the subtropical region during summer months, regardless of the wind field (Roden, 1974).

c. The field of net evaporative flux

This field is significant, because it leads to the establishment of primary salinity gradients in the ocean upon which the flow field acts to create or destroy salinity fronts. Net evaporation is the difference between evaporation and precipitation. Evaporation can be estimated from a knowledge of the vapor pressure difference and the wind speed. The former depends upon the difference between the sea and dewpoint temperatures in a nonlinear fashion. For a given wind speed and sea-dewpoint temperature difference, evaporation in the tropics is four times larger than in polar regions. Therefore, small temperature differences in low latitudes can have as large an effect on turbulent heat transfer to the atmosphere as do large temperature differences in high latitudes. In the ocean, areas of high evaporation are related to large downward salt and buoyancy fluxes (Agafonova *et al.*, 1972; Monin, 1972).

The seasonal variation of the evaporation-precipitation difference is shown in Fig. 14, which is based on wind speeds and sea temperatures by the National Marine Fisheries Service (1948–67), dewpoint temperatures by Crutcher and Meserve (1970), and precipitation maps by Taylor (1973). Positive net evaporation prevails south of 34°N and negative net evaporation

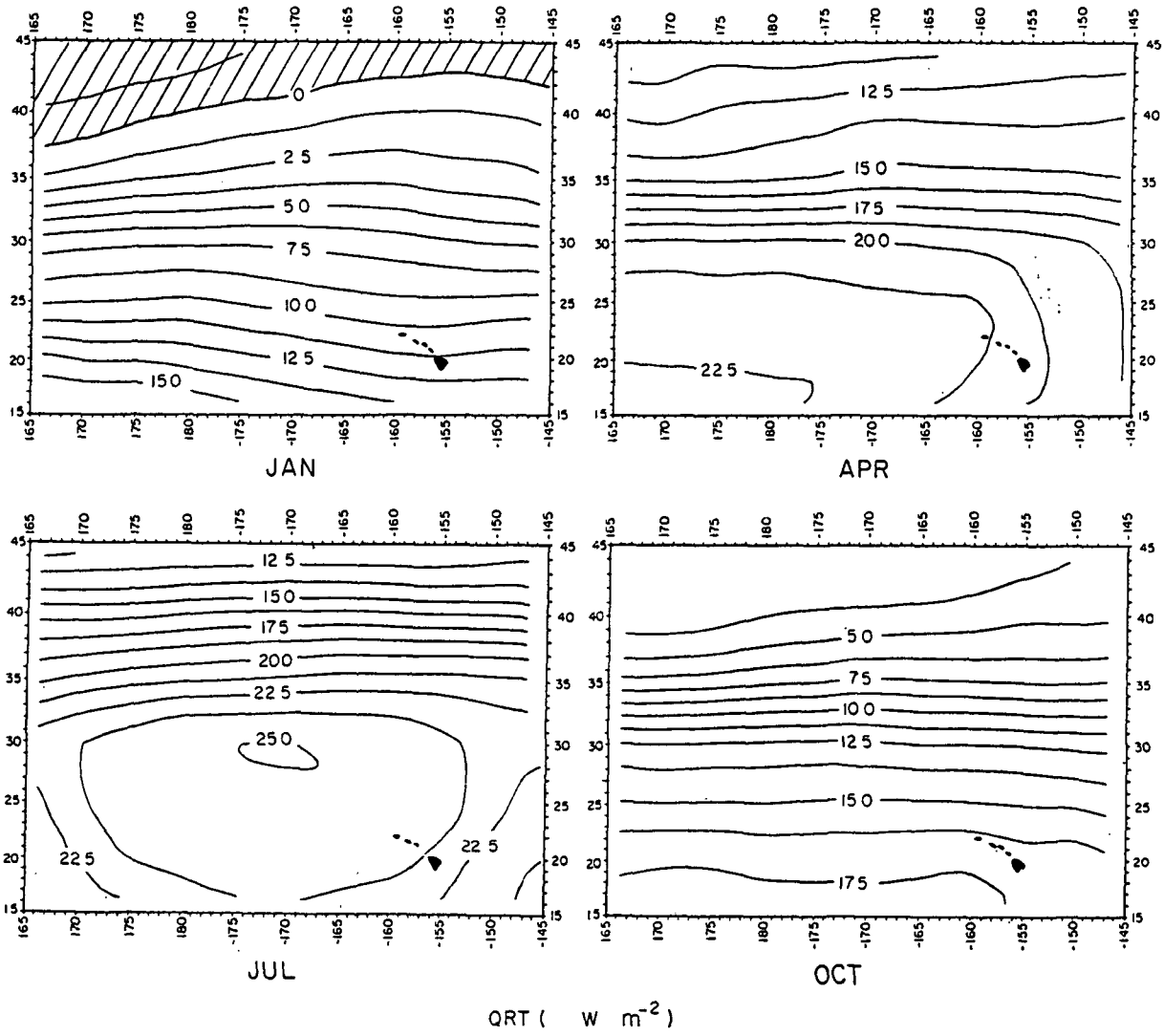

FIG. 13. Seasonal variation of the spatial distribution of the net radiative heat flux into the ocean on a 1° latitude-longitude grid based on satellite cloud cover observations. Areas of radiative heat loss are hatched.

north of 43°N. The zero line undergoes a distinct seasonal variation, being furthest south in spring and furthest north in fall. The maximum of net evaporation also migrates with season, from the west in winter and spring, to the east in summer and fall.

Areas favorable for salinity frontogenesis can be outlined by superimposing the Ekman transport and net evaporation fields shown in Figs. 11 and 14. During winter the frontogenetic zone lies around latitude 23°N west of the Hawaiian islands and around 30°N east of these islands. During spring, salinity fronts are most likely to form between 30 and 35°N, and during summer and fall in the vicinity of 35°N. This has also been observed on various crossings of the subtropical transition zone aboard the *Thomas G. Thompson* (Roden, 1970, 1972).

4. Kinematic aspects of surface fronts

Since particle convergence is often observed in frontal zones, it is instructive to look at the main relationships among fronts and particle trajectories. Only a few simple fields of motion will be considered here; for a fuller discussion of trajectory determinations, reference is made to Gordon and Taylor (1975).

a. Stationary geostrophic flow field

In this simple case, the particle trajectories are along isobars. A typical pressure configuration leading to frontogenesis is shown in Fig. 15 (top). The ellipses refer to low (L) and high (H) pressure cells, the black arrows indicate the flow of cold water, and the light arrows denote the flow of warm water. A temperature

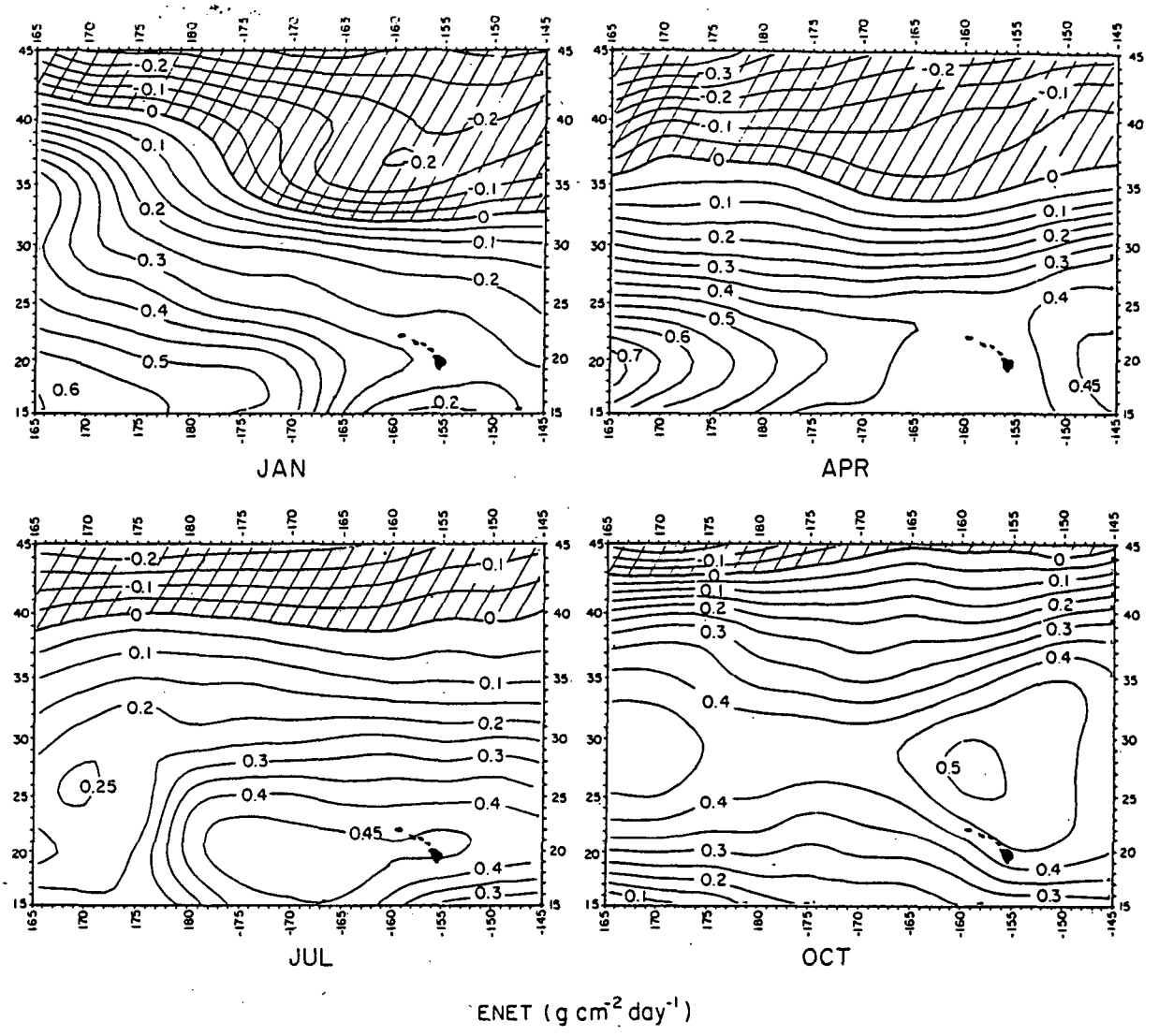

FIG. 14. Seasonal variation of the spatial distribution of net evaporation on a 1° latitude-longitude grid. Areas where precipitation exceeds evaporation are hatched.

front will form in the col region between the pressure cells and will be oriented from southwest to northeast, approximately. Such geostrophic fronts are common in the atmosphere (Palmén and Newton, 1969) and can be expected to be present in the ocean, below the upper mixed layer.

b. Stationary Ekman flow field

Here, the upper mixed layer moves at right angles to the surface wind stress. If the stress of the geostrophic wind is used, the water will move also at right angles to the isobars at the sea surface. This is shown in Fig. 15 (middle), where ellipses refer to atmospheric high and low pressure cells and the dark and light arrows denote cold and warm water, as before. A temperature front will form in the col region and will be oriented from west to east. Fronts of this type are common in the ocean and have been observed in the mid-Pacific (Roden, 1972, 1974).

The above discussion assumes that the particles move without heat gain or heat loss. Actually, equatorward moving particles will gain heat and poleward moving particles will lose heat. The effect of this is a lessening of the temperature contrast in the particle convergence zone. In some cases of sluggish motion and strong heating or cooling, the temperature contrast in the particle convergence zone will be eliminated completely. When this happens, temperature fronts and particle confluence zones will not coincide. Such a case is shown in Fig. 15

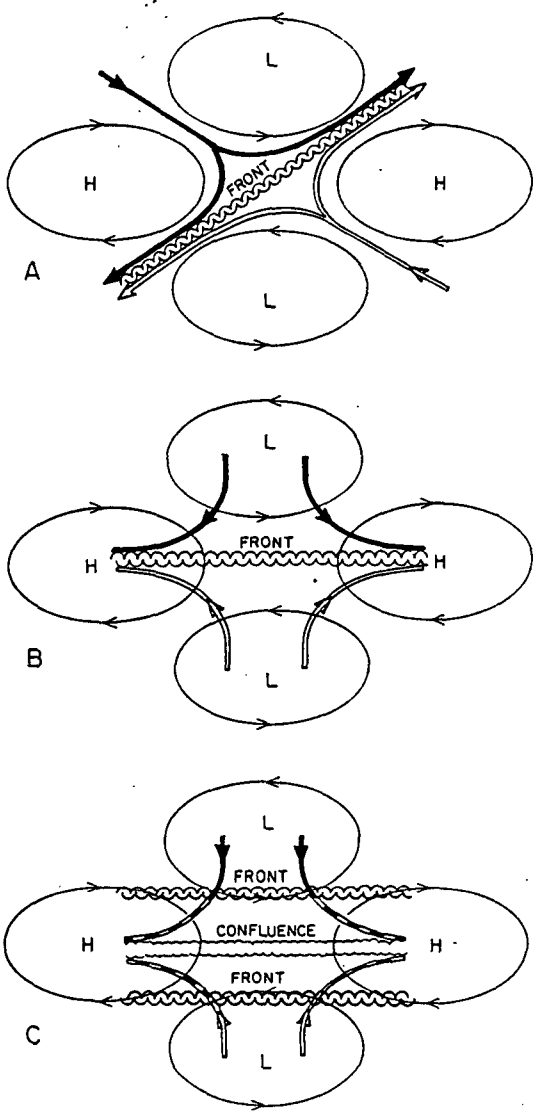

FIG. 15. Frontogenesis due to (A) convergence in the geostrophic flow field when temperature is conservative, (B) convergence in the surface Ekman transport field when temperature is conservative, and (C) convergence in the surface Ekman transport field when the temperature is nonconservative. Ellipses indicate pressure, dark arrows cold water, and light arrows warm water.

(bottom). As before, particle confluence due to Ekman transport occurs in the col region between the pressure cells. Temperature fronts are retarded relative to particle confluence, however, because heat exchange with the environment during particle motion has decreased and finally eliminated the original temperature contrast (checkered arrows). Observations from the ocean are lacking, but the phenomenon has been observed in the atmosphere (Pettersen, 1956).

d. Fronts associated with moving circular pressure disturbances

When the motion is nonstationary, fronts will be associated with particle rather than with streamline convergence. This involves calculations of the trajectories of individual particles which, in general, is a difficult task. Some insight can be gained, however, by considering an idealized case in which a pair of concentric pressure disturbances moves at constant speed in an initially zonal temperature field. When the current speed is larger than the speed of propagation of the pressure disturbances, the curvature of the trajectories is in the same sense as the isobars. This is shown in Fig. 16, where the concentric circles indicate the pressure pattern at initial time and the arrows indicate the particle trajectories. The dots refer to particle positions at successive time intervals. Particles located at the rear of the travelling pressure disturbance are displaced furthest and those located in front are displaced least. When the low pressure is poleward of the high pressure, a temperature front forms between. This front will be strongest behind the travelling pressure disturbances, because particles with long trajectories from opposite directions converge upon each other. No temperature front is formed when the high pressure is poleward of the low pressure, because the particle trajectories diverge.

5. Main thermodynamic aspects of fronts

For the following discussion, it is useful to decompose the instantaneous variables into mean and fluctuating parts and to define fronts in terms of the maximum magnitude of the average gradient. From a physical point of view, the interest is in processes that lead to time changes in the intensity of average fronts.

Starting with the equations for heat and salt conservation, averaging, applying the gradient operator, and assuming that the radiative and turbulent energy fluxes take place in the vertical direction predominantly, and

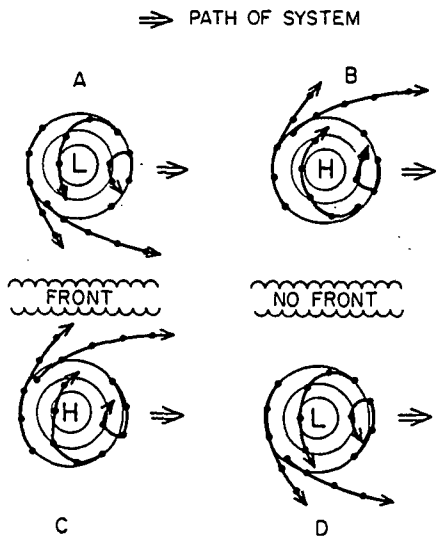

FIG. 16. Frontogenesis associated with circular eastward moving pressure systems (A–D). Dots indicate particle positions at successive time intervals.

neglecting molecular processes because of their smallness, one obtains the following for the local time change of the temperature and salinity fronts, respectively:

$$\frac{\partial}{\partial t}|\nabla\bar{\theta}| = -\left[\frac{\partial \bar{v}_{n\theta}}{\partial n}|\nabla\bar{\theta}| + \bar{v}_{n\theta}\frac{\partial|\nabla\bar{\theta}|}{\partial n} + \frac{\partial}{\partial n}\left(\frac{1}{\rho c_{vs}}\frac{\partial \bar{q}_z}{\partial z}\right) + \frac{\partial}{\partial n}\left(\frac{1}{\bar{\rho}\bar{c}_{vs}}\frac{\partial}{\partial z}\bar{\rho}\bar{c}_{vs}\langle w'\theta'\rangle\right)\right], \quad (1)$$

$$\frac{\partial}{\partial t}|\nabla\bar{S}| = -\left[\frac{\partial \bar{v}_{ns}}{\partial n}|\nabla\bar{S}| + \bar{v}_{ns}\frac{\partial|\nabla\bar{S}|}{\partial n} + \frac{\partial}{\partial n}\left(\frac{10^{-3}}{\rho}\frac{\partial \bar{r}_z}{\partial z}\right) + \frac{\partial}{\partial n}\left(\frac{1}{\bar{\rho}}\frac{\partial}{\partial z}\bar{\rho}\langle w'S'\rangle\right)\right], \quad (2)$$

where the barred quantities refer to the mean values and the primes to the turbulent fluctuations; θ is potential temperature (K), S salinity (g kg^{-1}), t time, and $v_{n\theta}$ and v_{ns} are the velocity components normal to the temperature and salinity fronts, respectively, the normals being denoted by n and taken in direction of increasing values; ρ is density, c_{vs} specific heat of sea water at constant volume and salinity, w the vertical velocity, q_z the vertical component of the radiative heat flux, and r_z the vertical component of the nonturbulent salt flux, all taken positive upward.

The terms on the right-hand side of (1) and (2) describe the various processes affecting frontal dynamics. These are, in sequence: (i) velocity convergence in a region of existing thermohaline gradients; (ii) advection of temperature and salinity gradients; (iii) geographically nonuniform radiative heat and nonturbulent salt fluxes; and (iv) geographically nonuniform turbulent heat and salt fluxes.

Term (i) is particularly large in regions of confluence, where currents of different origin meet. This happens not only at the confluence of the Kuroshio-Oyashio and the California and north equatorial current systems, but also in mid-ocean, where the geostrophic currents are weak, namely, along convergence zones of the wind-induced Ekman transport. Term (ii) vanishes by definition, because at the front the gradient is assumed to have a maximum. Term (iii) involves the radiative heat flux and fresh water flux (due to precipitation) and is important in the upper layers of the ocean only. This term is large at the boundaries of planetary wind systems, where cloudiness and precipitation fronts are often located. Term (iv) is significant in the turbulent regions of the ocean. At the sea-air interface it is related to evaporative and conductive fluxes (Montgomery, 1948) and is large in regions of planetary wind and moisture boundaries. Below the sea surface, the magnitude of this turbulent flux term is not well known. It can be expected to be large in the upper ocean and have a minimum in the high stability layer, where turbulence is surpressed.

Approximate magnitudes of the terms in (1) and (2) are given in Table 2 for various fronts of the central Pacific. It appears that for time scales of 10^5 s ($\sim$1 day) and horizontal length scales of 10^5 m ($\sim$100 km), the velocity convergence term dominates at the northern fronts (Kuroshio, subarctic), while at the lower latitude fronts (subtropical, doldrum) all terms are of comparable magnitude.

The local time changes of sound velocity and density fronts can be derived from (1) and (2) and a knowledge of the empirically determined equation of state (Fofonoff, 1962) and the sound velocity equation (Vigoureux and Hersey, 1962; Tolstoy and Clay, 1966). For the time change of the magnitude of the sound velocity front and density fronts, respectively, one has

$$\frac{\partial}{\partial t}|\nabla\bar{c}| \approx \frac{\partial}{\partial t}|4.6\nabla\bar{T} + 1.4\nabla\bar{S} + 0.016\nabla\bar{P}|, \quad (3)$$

$$\frac{\partial}{\partial t}|\nabla\bar{\rho}| \approx \frac{\partial}{\partial t}|-1.5\times10^{-4}\nabla\bar{T} + 7.7\times10^{-4}\nabla\bar{S} + 4.5\times10^{-6}\nabla\bar{P}|, \quad (4)$$

where c is sound velocity (m s^{-1}), T sea temperature (°C), S salinity (‰), and P pressure (db).

For horizontal terms, the pressure terms are negligible. In the open ocean, temperature differences across a front reach 10°C, while salinity differences are usually less than 2‰. Oceanic sound velocity fronts can therefore be described in terms of temperature fronts. Oceanic density fronts, on the other hand, cannot be so described, because when the temperature and salinity fronts point in the same direction, no density front need result (Fig. 7). In more restricted regions, such as off river estuaries and in areas of ice melt, salinity differences across the salt water-fresh water interface may reach 30‰, completely masking the temperature differences. Here, sound velocity and density fronts are closely associated with salinity fronts.

In the atmosphere, baroclinic jets are often found at fronts (Palmén and Newton, 1969). In the ocean, baroclinic jets may or may not accompany fronts, depending upon whether or not the temperature and salinity fronts compensate each other. An expression for local time change of baroclinic flow magnitude can be obtained from the vertically integrated continuity equation

$$\frac{\partial}{\partial t}\left|\nabla_H\int_{-h}^{\zeta}\bar{\rho}dz\right| = -\frac{\partial}{\partial n}[\nabla_H\cdot\bar{\mathbf{M}}_H + \bar{a}\bar{c}_{ps}^{-1}(\bar{Q}_r+\bar{Q}_t) + 10^{-3}\bar{S}(\bar{E}-\bar{R}) + \bar{a}\bar{R}(\bar{T}-\bar{T}_r)], \quad (5)$$

where the normal n points in the direction of the integrated density front; $-h$ is the sea bottom, ζ the sea surface, $\mathbf{M}_H$ the total horizontal mass transport, a the coefficient of thermal expansion, and c_{ps} the specific heat

TABLE 2. Estimated magnitudes of the terms in Eqs. (1) and (2). The estimates are for horizontal fronts and are based on time scales of 10^6 s and horizontal scales of 10^5 m. At the front, the magnitude of the gradient is assumed to have a maximum so that the second right-hand terms in (1) and (2) vanish by definition.

Term	Kuroshio front	Subarctic front	Subtropical front	Doldrum front
	Temperature fronts (all units, °C m^{-1} s^{-1})			
$-\frac{\partial \bar{V}_{n\theta}}{\partial n}\lvert\nabla\bar{\theta}\rvert$	12×10^{-11}	6×10^{-11}	3×10^{-11}	1×10^{-11}
$-\frac{\partial}{\partial n}\left(\frac{1}{\bar{\rho}\bar{c}_{ve}}\frac{\partial qz}{\partial z}\right)$	6×10^{-12}	6×10^{-12}	1×10^{-11}	-1×10^{-11}
$-\frac{\partial}{\partial n}\left(\frac{1}{\bar{\rho}\bar{c}_{ve}}\frac{\partial}{\partial z}\bar{\rho}\bar{c}_{ve}\langle w'\theta'\rangle\right)$	-2×10^{-12}	-2×10^{-12}	-5×10^{-12}	7×10^{-12}
$\frac{\partial}{\partial t}\lvert\nabla\bar{\theta}\rvert$*	12.4×10^{-11}	6.4×10^{-11}	3.5×10^{-11}	7×10^{-12}
	Salinity fronts (all units, ‰ m^{-1} s^{-1})			
$-\frac{\partial \bar{V}_{ns}}{\partial n}\lvert\nabla\bar{S}\rvert$	2×10^{-12}	1×10^{-12}	5×10^{-13}	1×10^{-12}
$-\frac{\partial}{\partial n}$	1×10^{-13}	1×10^{-13}	1×10^{-13}	2×10^{-13}
$-\frac{\partial}{\partial n}\left(\frac{1}{\bar{\rho}}\frac{\partial}{\partial z}\bar{\rho}\langle w'S'\rangle\right)$	1×10^{-13}	1×10^{-13}	2×10^{-13}	3×10^{-13}
$\frac{\partial}{\partial t}\lvert\nabla\bar{S}\rvert$*	2.2×10^{-12}	1.2×10^{-12}	8×10^{-13}	1.5×10^{-12}

* Sum of the above.

of sea water at constant pressure and salinity; Q_r and Q_t are the radiative and turbulent heat fluxes, positive upward, E and R the evaporation and rainfall rates in mass units, positive upward, T and T_r the temperatures of the sea surface and of rain, and S is the salinity (‰).

Baroclinic jets will tend to form when the right-hand side of (5) is positive. This implies both total mass transport convergence and surface energy flux convergence. The observed fronts are most intense in the upper ocean and often show strong affinity to Ekman transport convergence lines, rather than to total transport convergence lines. Because of this, baroclinic jets are often some distance from the surface manifestation of the temperature and salinity fronts. This has been observed at both the subtropical and doldrum fronts (Figs. 8–10).

According to (5) baroclinic jets could also form in the absence of mass transport convergence and be related to convergence lines in the surface energy fluxes. Whether this actually happens is not known.

6. Conclusions

The following conclusions can be drawn from an examination of the main oceanic fronts of the North Pacific and from a study of frontogenetic processes:

1) Fronts are features of the upper ocean and form near mass transport and energy flux convergence lines.

2) Frontogenesis in the upper layers of the ocean is strongly dependent upon the configuration of the wind stress field.

3) Temperature and salinity fronts in the upper layer of the ocean are not necessarily coincident.

4) When the temperature and salinity fronts are coincident and point in the same direction, density fronts do not occur.

5) During periods of strong and persistent winds, the upper and lower parts of the front separate by as much as 200 km, with the depth of separation at the pycnocline. This suggests Ekman-type displacement of the upper mixed layer.

6) In the confluence region between the Kuroshio and Oyashio multiple temperature and salinity fronts with a horizontal spacing of 60–70 km have been observed, which is suggestive of baroclinic Rossby waves.

7) Not all temperature and salinity fronts are accompanied by strong baroclinic flow. In the mid-Pacific, thermohaline fronts occur along Ekman transport convergence lines, while the strongest baroclinic flow is found along total transport convergence lines. The horizontal distance between these convergence lines may exceed 200 km.

Acknowledgments. I am indebeted to M. Rattray and P. Welander for fruitful discussions. C. A. Barnes, R. H. Fleming and L. H. Larsen offered advice, M. Johnson coordinated the field work, and M. Yang and P. Yuan

carried out the programming and calculations. The scientific and operational crew of the *Thomas G. Thompson*, Captains R. Schelling and C. Clampitt commanding, are to be commended for outstanding performance under difficult weather conditions. The research reported herein was supported by the Office of Naval Research under Contract N-00014-75-C-0502 Project NR 083-012.

REFERENCES

Agafonova, E. G., L. I. Galerkin and A. S. Monin, 1972: Origin of the thermohaline circulation of the ocean. *Oceanology*, 12, 790–795.

Budyko, M. I., 1974: *Climate and Life*. Academic Press, 508 pp.

Charney, J., 1971: Tropical cyclogenesis and formation of the intertropical convergence zone. *Mathematical Problems in the Geophysical Sciences, Lectures in Applied Mathematics*, Vol. 13, Amer. Math. Soc., 355–368.

Crutcher, H. L. and J. M. Meserve, 1970: Selected level heights, temperature, and dewpoints for the northern hemisphere. U. S. Government Printing Office, Washington, D. C. 20402.

Dodimead, A. J., F. Favorite and T. Hirano, 1963: Review of the oceanography of the subarctic Pacific region. *Intern. North Pacific Fish. Comm. Bull.*, No. 13, 195 pp.

Fofonoff, N. P., 1962: Physical properties of sea water. *The Sea*, Vol. 1, M. N. Hill, Ed., Interscience, 3–30.

Godske, C. L., T. Bergeron, J. Bjerknes and R. C. Bundgaard, 1957: *Dynamic Meterorology and Weather Forecasting*. Amer. Meteor. Soc., 800 pp.

Gordon, A. H. and R. C. Taylor, 1975: Computations of surface layer air parcel trajectories and weather in the oceanic tropics. *Intern. Indian Ocean Expedition Meteor. Monogr.*, No. 7, University Press of Hawaii, 112 pp.

Japan Meteorological Agency, 1970–74: Ten-day marine report (contoured charts of sea surface temperature for 10-day periods). Tokyo.

Kawai, H., 1972: Hydrography of the Kuroshio extension. *Kuroshio, Physical Aspects of the Japan Current*, H. Stommel and K. Yoshida, Eds., University of Washington Press, 235–352.

Kondratyev, K. Ya., 1969: *Radiation in the Atmosphere*. Academic Press, 912 pp.

Longuet-Higgins, M. S., 1965: The response of a stratified ocean to stationary or moving wind systems. *Deep-Sea Res.*, 12, 923–973.

Mazusawa, J., 1957: A contribution to the knowledge of the Kuroshio east of Japan. *Oceanogr. Mag.*, 9, 21–34.

Miller, D. B., 1971: *Global Atlas of Relative Cloud Cover 1967–70, Based on Data from Meteorological Satellites*. National Environmental Satellite Service, Washington, D. C., 273 pp.

Monin, A. S., 1972: Specific features of sea turbulence. *Rapports et Proces-Verbeaux des Reunions*, No. 162, *Conseil International pour l'Exploration de lar Mer*, Charlottenlund Slot, Denmark, 7–11.

Montgomery, R. B., 1948: Vertical eddy flux of heat in the atmosphere. *J. Meteor.*, 5, 265–274.

National Marine Fisheries Service, 1948–67: *Pacific Ocean Climatological Data Base* (magnetic tape). NMFS Southwest Fisheries Center, La Jolla, Calif.

National Weather Service, 1957–66: Monthly mean sea level atmospheric pressure maps for the Northern Hemisphere and listings of the monthly mean pressures at 5 degree latitude-longitude intersections. National Meteorological Center, Suitland, Md.

Palmén, E., and C. W. Newton, 1969: *Atmospheric Circulation Systems*. Academic Press, 602 pp.

Pedlosky, J., 1971: Geophysical fluid dynamics. *Mathematical Problems in the Geophysical Sciences, Lectures in Applied Mathematics*, Vol. 13, Amer. Math. Soc., 1–60.

Pettersen, S., 1956: *Weather Analysis and Forecasting*, Vol. 1. McGraw Hill, 428 pp.

Roden, G. I., 1970: Aspects of the mid-Pacific transition zone. *J. Geophys. Res.*, 75, 1097–1109.

——, 1972: Temperature and salinity fronts at the boundaries of the subarctic and subtropical transition zone in the western Pacific. *J. Geophys. Res.*, 77, 7155–7187.

——, 1974: Thermohaline structure, fronts, and sea-air energy exchange of the trade wind region east of Hawaii. *J. Phys. Oceanogr.*, 4, 168–182.

Schaefer, J. T., 1974: A simulative model of dryline motion. *J. Atmos. Sci.*, 31, 956–964.

Taft, B. A., 1972: Characteristics of the flow of the Kuroshio south of Japan. *Kuroshio, Physical Aspects of the Japan Current*, H. Stommel and K. Yoshida, Eds., University of Washington Press, 165–216.

Tareev, B. A., 1965: Unstable Rossby waves and the instability of oceanic currents. *Izv. Atmos. Oceanic Phys.*, 1, 426–438.

Taylor, R. C., 1973: *An Atlas of Pacific Islands Rainfall*. Hawaii Institute of Geophysics Data Report, No. 25.

Tolstoy, I., and C. S. Clay, 1966: *Ocean Acoustics*. McGraw Hill, 293 pp.

Uda, M., 1935: The results of simultaneous oceanographical investigations of the North Pacific Ocean adjacent to Japan. *Jap. Imp. Fish. Res. Exp. Sta.*, 6, 1–130.

——, 1938: Researches on "siome" or current rip in the seas and oceans. *Geophys. Mag.*, 11, 307–372.

——, 1963: Oceanography of the subarctic Pacific Ocean. *J. Fish. Res. Bd. Can.*, 20, 119–179.

——, and K. Hasunuma, 1969: The eastward subtropical countercurrent in the western North Pacific Ocean. *J. Oceanogr. Soc. Jap.*, 25, 201–210.

Van Mieghem, J. M., 1951: Hydrodynamic instability. *Compendium of Meteorology*, Amer. Meteor. Soc., 434–453.

Vigoureux, P., and J. B. Hersey, 1962: Sound in the sea. *The Sea* Vol. 1, M. N. Hill, Ed., Interscience, 476–497.

Yoshida, K., and T. Kidōkoro, 1967: A subtropical countercurrent (II), a prediction of eastward flows at lower subtropical latitudes. *J. Oceanogr. Soc. Jap.*, 5, 231–246.